NEURAL REGENERATION RESEARCH
www.nrronline.org

Research Article

Anodal transcranial direct current stimulation alleviates cognitive impairment in an APP/PS1 model of Alzheimer's disease in the preclinical stage

https://doi.org/10.4103/1673-5374.337053

Date of submission: August 9, 2021

Date of decision: November 4, 2021

Date of acceptance: December 17, 2021

Date of web publication: February 28, 2022

Yin-Pei Luo[1, 2], Zhi Liu[3], Cong Wang[2], Xiu-Fang Yang[2], Xiao-Ying Wu[2], Xue-Long Tian[2], Hui-Zhong Wen[1, *]

From the Contents

Graphical Abstract *Long-term effects of anodal transcranial direct current stimulation (AtDCS) in the preclinical-stage APP/PS1 double transgenic mice*

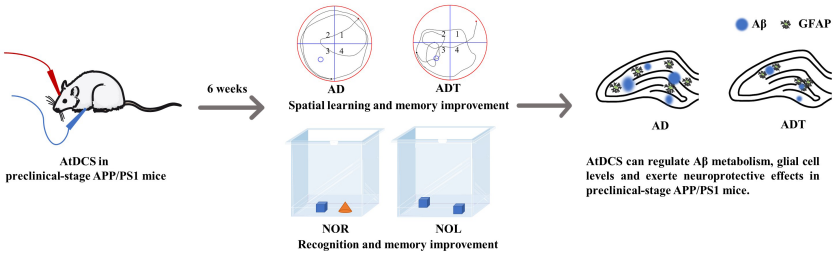

Abstract

Anodal transcranial direct current stimulation (AtDCS) has been shown to alleviate cognitive impairment in an APP/PS1 model of Alzheimer's disease in the preclinical stage. However, this enhancement was only observed immediately after AtDCS, and the long-term effect of AtDCS remains unknown. In this study, we treated 26-week-old mouse models of Alzheimer's disease in the preclinical stage with 10 AtDCS sessions or sham stimulation. The Morris water maze, novel object recognition task, and novel object location test were implemented to evaluate spatial learning memory and recognition memory of mice. Western blotting was used to detect the relevant protein content. Morphological changes were observed using immunohistochemistry and immunofluorescence staining. Six weeks after treatment, the mice subjected to AtDCS sessions had a shorter escape latency, a shorter path length, more platform area crossings, and spent more time in the target quadrant than sham-stimulated mice. The mice subjected to AtDCS sessions also performed better in the novel object recognition and novel object location tests than sham-stimulated mice. Furthermore, AtDCS reduced the levels of amyloid-β42 and glial fibrillary acidic protein, a marker of astrocyte activation, and increased the level of neuronal marker NeuN in hippocampal tissue. These findings suggest that AtDCS can improve the spatial learning and memory abilities and pathological state of an APP/PS1 mouse model of Alzheimer's disease in the preclinical stage, with improvements that last for at least 6 weeks.

Key Words: Alzheimer's disease; amyloid-β; anodal transcranial direct current stimulation; cognitive function; inflammation; long-term effect; neuron; preclinical stage

Introduction

Alzheimer's disease (AD) is mainly characterized by progressive memory and cognitive decline, and its main pathological hallmarks include neurofibrillary tangles, amyloid plaques (abnormal deposition of amyloid-β (Aβ)) and neuronal loss (Jack et al., 2018; Aranda et al., 2021; Patwardhan and Belemkar, 2021). It may take up to 20 years or longer after the initiation of AD pathophysiology for clinical symptoms to appear (Villemagne et al., 2013; Porsteinsson et al., 2021). The irreversibility and long prodromal period of AD have prompted researchers to shift their attention from the clinical stage to the preclinical stage for the treatment of AD (Ryan and Rossor, 2011; Villemagne et al., 2013).

Anodal transcranial direct current stimulation (AtDCS) is a safe, noninvasive brain stimulation treatment. AtDCS provides a constant direct current to a target area of the brain through an anode electrode during stimulation, and the generated constant electric field penetrates the skull to increase the excitability of the neurons; after stimulation, a cumulative effect (long-term effect) that alters the levels of various neurotransmitters and dynamically regulates synaptic plasticity in the brain can be observed (Nitsche and Paulus, 2000; Stagg and Nitsche, 2011). AtDCS has been found to improve memory and cognition in patients and animal models in the clinical stage of AD, with sustained treatment effects (Lu et al., 2019; Yang et al., 2019; Gangemi et al., 2021). AtDCS has also been reported to improve spatial learning and memory in animal models in the preclinical stage of AD (Luo et al., 2020). However, to date, there have been no studies on the long-term effect of AtDCS in the preclinical stage of AD.

Abnormal Aβ deposition occurs throughout the course of AD (Sperling et al., 2011; Lee et al., 2019; Mycroft-West et al., 2020; Gutierrez et al., 2021; Wang et al., 2021), and the formation of Aβ deposits is mainly regulated by the production and degradation of Aβ (Chen et al., 2017; Patwardhan and Belemkar, 2021). In patients with AD and animal models of AD, the levels of proteins associated with Aβ metabolism have been reported to be abnormal (Sun et al., 2019; Patwardhan and Belemkar, 2021; Porsteinsson et al., 2021). In the pathological process of AD, the continuous increase in the Aβ level is also accompanied by abnormal changes in astrocytes (Zhu et al., 2017). Normal astrocytes participate in the degradation and clearance of Aβ and protect neurons, but when the degradation and clearance of Aβ are insufficient, activated astrocytes release excess glutamate, induce neuronal excitotoxicity and an inflammatory cascade, and participate in the generation of endogenous Aβ, which in turn promotes the progression of AD (Nitsche and Paulus, 2000; Carter et al., 2019; Martorell et al., 2019). Highly neurotoxic Aβ can also cause neuronal cell death through autocrine/paracrine

[1]Chongqing Key Laboratory of Neurobiology, Department of Neurobiology, School of Basic Medicine, Army Medical University, Chongqing, China; [2]Chongqing Medical Electronics Engineering Technology Research Center, Laboratory of Neural Regulation and Rehabilitation Technology, College of Bioengineering, Chongqing University, Chongqing, China; [3]Department of Histology and Embryology, School of Basic Medicine, Army Medical University, Chongqing, China
*Correspondence to: Hui-Zhong Wen, PhD, justzhong@sina.com.
https://orcid.org/0000-0001-5590-4275 (Hui-Zhong Wen); https://orcid.org/0000-0002-2971-7529 (Xue-Long Tian)

Funding: *This study was supported by the National Natural Science Foundation of China, No. 31971287 (to XYW) and the Advanced Interdisciplinary Studies Foundation of School of Basic Medical Science, Army Medical University of China, No. 2018JCQY07 (to HZW).*
How to cite this article: *Luo YP, Liu Z, Wang C, Yang XF, Wu XY, Tian XL, Wen HZ (2022) Anodal transcranial direct current stimulation alleviates cognitive impairment in an APP/PS1 model of Alzheimer's disease in the preclinical stage. Neural Regen Res 17(10):2278-2285.*

mechanisms through the production of proinflammatory cytokines, which is mainly triggered by signal transduction pathways in astrocytes (Hughes et al., 2020). The role of astrocytes in AD is being increasingly recognized (Verkhratsky et al., 2010; Fakhoury, 2018). In animal models of AD, AtDCS has been shown to reduce Aβ and astrocyte levels, and protect neurons (Yu et al., 2015; Luo et al., 2020). However, there is still a lack of research on the regulatory effect of AtDCS on Aβ metabolism and its neuroprotective effects in the preclinical stage of AD.

Amyloid precursor protein/presenilin-1 (APP/PS1) double transgenic mice are often used as transgenic animal models of AD, as they can simulate the process of AD in terms of Aβ metabolism, neuroinflammation, and cognitive deficits (Esquerda-Canals et al., 2017; Zhu et al., 2017; Sun et al., 2019). In this study, we studied the long-term effect of AtDCS in APP/PS1 (B6/J-Tg (APPswe, PSEN1dE9)) mice in the preclinical stage of AD, and explore the mechanism underlying its effect on Aβ metabolism, astrocytes, and neuroprotection.

Materials and Methods

Animals

This randomized animal experiment was approved by the Laboratory Animal Welfare and Ethical Committee of the Army Medical University (approval No. AMUWEC20191829) on June 20, 2019. Seventeen-week-old APP/PS1 (n = 33) and C57BL/6J (C57) mice (n = 11) from the Model Animal Research Center of Nanjing University (animal license No. SCXK (Su) 2012-0007) were housed at a temperature of 20–22°C on a 12-hour light/dark cycle with sufficient food and water for 9 weeks. All mice were male, with a weight range of 25–30 g. Male mice were chosen to reduce the influence of sex hormones, considering the sex-dependency of AD (Radaghdam et al., 2021). All experiments were designed and reported according to the Animal Research: Reporting of *In Vivo* Experiments (ARRIVE) guidelines (Percie du Sert et al., 2020).

Study design

The APP/PS1 mice were randomly divided into the APP/PS1 (AD), APP/PS1 + sham AtDCS (ADS), and APP/PS1 + AtDCS (ADT) groups. C57 mice were used as the control group (CTL group). There were 11 mice in each group. ADT group mice were treated with AtDCS for 2 weeks beginning at 26 weeks of age. Each week of treatment involved five consecutive days of AtDCS followed by a two-day interval. The protocol was based on the application of tDCS in mice (Pikhovych et al., 2016). When all mice were 34 weeks old, the Morris water maze, novel object recognition test, and novel object location test were implemented to evaluate spatial learning and memory and recognition memory. Then, western blot, immunohistochemistry, and immunofluorescence were performed to evaluate changes in the hippocampus in the CTL, AD, and ADT groups (**Figure 1**). The evaluator was blind to the grouping.

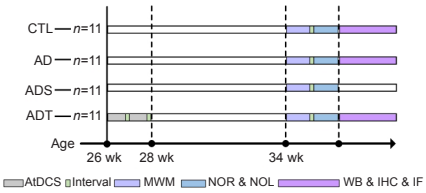

Figure 1 | **Experimental design.**
AtDCS was applied for five consecutive days per week followed by a 2-day interval, for 2 weeks. At the age of 34 weeks, all mice were sequentially subjected to the MWM, NOR, and NOL tests. Finally, WB, IHC, and IF were performed for histological evaluation of the hippocampus. AD: APP/PS1; ADS: APP/PS1 + sham AtDCS; AtDCS: Anodal transcranial direct current stimulation; ADT: APP/PS1 + AtDCS; APP/PS1: APPswe/PSEN1dE9; CTL: control; IF: immunohistochemistry; IHC: immunohistochemistry; MWM: Morris water maze; NOL: novel object location; NOR: novel object recognition; WB: Western blot.

AtDCS

All mice underwent electrode implantation surgery, as described previously, on the day before AtDCS (Yu et al., 2015; Luo et al., 2020). The mice received inhalation of 3% isoflurane (Shenzhen Reward Life Science Co., Ltd., Shenzhen, China) for anesthesia induction, and 0.8–1.5% for anesthesia maintenance. Then, mice were fixed in a stereotaxic apparatus (Shenzhen Reward Life Science Co., Ltd.). A heating blanket maintained the body temperature at 37.0 ± 0.5°C. The scalp of each mouse was incised to expose the skull, and then the skull was positioned horizontally. A laboratory-made circular polyvinyl chloride anode electrode filled with cotton and copper wire with a diameter of 2 mm was adhered onto the skull over the frontal cortex (**Figure 2**) using nontoxic glass ionomer cement (Changshu Shang Dental Materials Co., Ltd., Changshu, China). The cathode electrode was a round silver chloride electrocardiogram electrode with a diameter of 2 cm that was attached to the chest and abdomen of the mice. Twenty-four hours after surgery, AtDCS was performed in the ADT group (150 μA, 30 minutes/day). The ADS group received sham stimulation (150 μA, 10 seconds/day). Mice could move freely during AtDCS and sham AtDCS. Before each AtDCS session, the anode electrode was wetted with physiological saline. A multimeter (Double King Industrial Holdings Co., Ltd. Shenzhen, China) monitored the current during AtDCS.

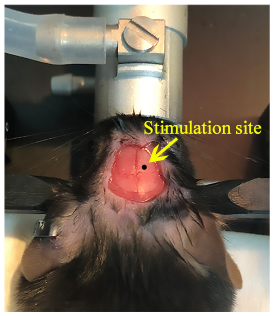

Figure 2 | **Stimulation site of AtDCS.**
The stimulation site (arrow) of AtDCS was anteroposterior: +1.0 mm, mediolateral: +1.5 mm. AtDCS: Anodal transcranial direct current stimulation.

Morris water maze test

The spatial learning and memory abilities of the mice were assessed at the age of 34 weeks using the Morris water maze test, as described in previous work (Bello-Arroyo et al., 2018). The Morris water maze (Shanghai XinRuan Information Technology Co., Ltd., Shanghai, China) consisted of a circular pool (diameter: 120 cm; height: 90 cm; temperature: 22 ± 1°C) and a circular platform (diameter: 12 cm). For black APP/PS1 mice, nontoxic white dye was added to the pool and mixed well with the water. Dark curtains surrounded the pool. Markers of different shapes and colors were placed above the pool as spatial cues. The pool was divided into four quadrants. The platform was placed in the center of the third quadrant (target quadrant) of the pool. Mice were tested in the Morris water maze over 6 days.

In the visible platform test (day 1), the platform was 1 cm above the water. The mice were placed within any two quadrants of the pool, and the time to reach the platform (escape latency) and path length were recorded for 60 seconds. If the mouse did not find the platform within 60 seconds, it was guided to the platform and stayed there for 5 seconds, and the escape latency was recorded as 60 seconds. The time interval between each quadrant test was 20 minutes. In the hidden platform test (days 2–5), the platform was hidden 1 cm below the water. As in the visible platform test, mice were placed into the pool from four quadrants, and their escape latency and path length were recorded. The order of the starting four quadrants was randomized every day and repeated for 4 days. The platform was removed in the probe test (day 6). The mice were put into the pool from the first quadrant, and the number of platform crossings and the time spent in each quadrant within 30 seconds were recorded. A quiet environment with constant light was maintained throughout the Morris water maze test.

Novel object recognition and novel object location tests

Two days after the end of the Morris water maze test, the novel object recognition and novel object location tests were implemented to test the recognition memory of mice. As mentioned in previous work (Antunes and Biala, 2012; Martorell et al., 2019), the novel object recognition test includes a habituation phase, familiarization period, and test period. During the 2-day habituation phase, mice were exposed to a white test area (25 cm × 25 cm × 32 cm) for 5 minutes every day. A familiarization and a test period were performed on the third day. In the familiarization period, two identical red cubes (2 cm × 2 cm × 2 cm) were placed opposite each other in the white test area, 5 cm from the wall. The mice explored the two objects freely for 5 minutes. After 1 hour, one of the red cubes was replaced with a yellow cone (1 cm × 1 cm × 2 cm) in the test period. The exploration time (the duration mice spent within 2 cm around the object) during which mice freely explored the two objects within 5 minutes was recorded. The location of the novel and familiar objects was counterbalanced in all experiments. The discrimination ratio (time spent exploring the novel object/(time spent exploring the novel object + time spent exploring the familiar object) × 100%) was used to evaluate the recognition memory of mice. After each test, the test area and objects were cleaned with 75% alcohol to remove the odor left by mice. The novel object recognition testing environment was kept quiet and constantly lit.

The novel object location test was performed using a procedure similar to that of the novel object recognition task. However, during the test period of the novel object location test, instead of being replaced with a yellow cone, one of the red cubes was moved to a novel position, that is, in the corner opposite the other object. The location index for the novel object location test was calculated as the time spent exploring the object in the novel location/(time spent exploring the object in the novel location + time spent exploring the object in the familiar location) × 100%.

Western blot assay

Western blotting assay was used for semi-quantitative analysis of markers related to Aβ metabolism, astrocytes, and neurons. After completing all behavioral tests, the mice in the CTL, AD, and ADT groups (n = 3 per group) were anesthetized by inhaling excessive isoflurane, as described above, and then euthanized by cervical dislocation. The hippocampal tissues were quickly removed on ice. An appropriate amount of mixture of radioimmunoprecipitation assay lysis buffer (P0013B, Beyotime, Shanghai, China) and phenylmethanesulfonyl fluoride (ST506, Beyotime) was added to the hippocampal tissue to make the tissue fully homogenized, and then tissues were centrifuged (approximately 8000 × g, 4°C, 15 minutes). The supernatants were used as samples, and the total protein concentration was measured with a bicinchoninic acid assay kit (P0012S, Beyotime). The proteins were diluted with protein loading buffer (P0015L, Beyotime),

subjected to sodium dodecyl sulfate-polyacrylamide gel electrophoresis, and transferred to polyvinylidene fluoride membranes. The membranes were blocked (room temperature, 2 hours) with 5% protein blocking solution (P0216, Beyotime), incubated with the primary antibody (4°C, 24 hours), washed five times (8 minutes/wash) with Tris-buffered saline with Tween-20 (ST825, Beyotime), and incubated with secondary antibody (37°C, 2 hours). Finally, the membranes were developed using the immobilon western chemiluminescent horseradish peroxidase substrate (WBKLS0100, Millipore, Burlington, MA, USA). The optical density of each band was measured using Quantum One software v4.6.2 (Bio-Rad, Hercules, CA, USA) and normalized to that of glyceraldehyde-3-phosphate dehydrogenase. The detailed antibody information is provided in **Table 1**.

Table 1 | **Antibody information**

Antibodies	Host species	Source	Catalog number	RRID No.	Concentration
Primary antibodies					
Anti-$A\beta_{42}$	Rabbit	Abcam, Cambridge, UK	ab201060	AB_2818982	1:1000 (WB), 1:200 (IHC), 1:2000 (IF)
Anti-NeuN	Rabbit	Millipore, Darmstadt, Germany	ABN78	AB_10807945	1:1000 (WB), 1:200 (IHC)
Anti-GFAP	Mouse	Cell Signaling Technology, Danvers, MA, USA	3670	AB_561049	1:1000 (WB), 1:200 (IHC), 1:2000 (IF)
Anti-APP	Rabbit	Solarbio, Beijing, China	K001592P	–	1:1000 (WB)
Anti-ADAM10	Rabbit	Abcam, Cambridge, UK	ab1997	AB_302747	1:1000 (WB)
Anti-CD10	Rabbit	Bioss, Beijing, China	bs-0527R	AB_10854297	1:1000 (WB)
Anti-IDE	Rabbit	Bioss, Beijing, China	bs-0018R	AB_10856467	1:1000 (WB)
Anti-BACE1	Rabbit	Bioss, Beijing, China	bs-0164R	AB_10857657	1:1000 (WB)
Anti-caspase 3	Rabbit	Proteintech, Rosemont, IL, USA	19677-1-AP	AB_10733244	1:1000 (WB)
Anti-GAPDH	Rabbit	Beyotime, Shanghai, China	AF1186	–	1:1000 (WB)
Secondary antibodies					
Goat anti-mouse IgG (H+L) [HRP]	Goat	ZSGB-BIO, Beijing, China	ZB-2305	AB_2747415	1:2000 (WB), 1:200 (IHC)
Goat anti-rabbit IgG (H+L) [HRP]	Goat	ZSGB-BIO	ZB-2301	AB_2747412	1:2000 (WB), 1:200 (IHC)
Anti-mouse IgG (H+L) [Alexa Fluor 594]	Goat	Cell Signaling Technology, Danvers, MA, USA	8890	AB_2714182	1:2000 (IF)
Anti-rabbit IgG (H+L) [Alexa Fluor 488]	Goat	Cell Signaling Technology, Danvers, MA, USA	4412	AB_1904025	1:2000 (IF)

$A\beta_{42}$: Amyloid-β42; ADAM10: a disintegrin and metalloprotease domain 10; APP: amyloid precursor protein; BACE1: β-site amyloid precursor protein cleaving enzyme 1; CD10: neprilysin; GAPDH: glyceraldehyde-3-phosphate dehydrogenase; GFAP: glial fibrillary acidic protein; HRP: horseradish peroxidase; IDE: insulin-degrading enzyme; IF: immunohistochemistry; IHC: immunohistochemistry; RRID: research resource identifiers; WB: Western blot.

Immunohistochemistry and immunofluorescence

The morphological changes of Aβ deposition, astrocytes, and neurons were observed using immunohistochemistry and immunofluorescence staining. After completing all the behavioral tests, mice from the CTL, AD, and ADT groups (n = 8 per group) were deeply anesthetized by intraperitoneal injection with 75 mg/kg pentobarbital sodium (Sinopharm Chemical Reagent Co., Ltd., Shanghai, China), and perfused with 0.9% physiological saline and 4% paraformaldehyde at 4°C. The whole brains were fixed using 4% paraformaldehyde, dehydrated by sucrose, and then frozen coronal mouse brain sections containing the hippocampal region (20 μm thick) were obtained using a cryostat (CM1900, Leica, Nussloch, Germany).

For immunohistochemistry, the target brain sections were washed with phosphate buffered saline (PBS; the concentration of PBS was 0.01 M unless otherwise specified) for 5 minutes; this was repeated three times, then sections were blocked with 3% H_2O_2 (room temperature, 30 minutes). The sections were washed three times with PBS (5 minutes/wash) and then blocked with 10% goat serum blocking solution (ZLI-9021, Zhongshan Biotech, Beijing, China) at 37°C for 30 minutes. Then, the sections were incubated with primary antibodies, including anti-$A\beta_{42}$, anti-glial fibrillary acidic protein (GFAP), and anti-NeuN (4°C, 24 hours). The sections were removed and washed with PBS three times (5 minutes/wash). The sections were incubated with a horseradish peroxidase-conjugated goat anti-mouse or anti-rabbit antibody (37°C, 1 hour), and then washed with PBS three times (5 minutes/wash). Finally, the sections were developed for 2 minutes using diaminobenzidine-enhanced development solution (ZLI-9018, Zhongshan Biotech) and mounted on glass slides. Hippocampal slides subjected to immunohistochemistry for $A\beta_{42}$, GFAP, and NeuN from each group of mice were photographed using an optical microscope (BX60, Olympus, Tokyo, Japan). Image-Pro Plus 6.0 software (Media Cybernetics, Bethesda, MD, USA) was used to measure the integrated optical density (IOD) of $A\beta_{42}$, GFAP, and NeuN in the hippocampus in each group. The detailed antibody information is provided in **Table 1**.

For Aβ/GFAP double immunofluorescence staining, brain sections were first washed with PBS three times (5 minutes/wash), and then blocked with 10% goat serum blocking solution (30°C, 30 minutes). Then, the sections were incubated with primary antibodies, including anti-Aβ and anti-GFAP antibodies (4°C, 24 hours). The sections were removed and washed with PBS three times (5 minutes/wash). The sections were then incubated with fluorescein isothiocyanate-conjugated goat anti-mouse IgG and Cy3-conjugated goat anti-rabbit IgG (37°C, 1 hour), counterstained with 4′,6-diamidino-2-phenylindole (D8417, Sigma-Aldrich, Poole, UK) (room temperature, 10 minutes), and then washed in PBS (three times, 5 minutes/wash). The sections were mounted using Fluoromount-G fluorescent mounting medium (0100-01, Southern Biotech, Birmingham, AL, USA) and stored in a dark box. Images of the sections subjected to immunofluorescence were taken using a laser scanning confocal microscope (Axio Obsever.Z1/7, Zeiss, Jena, Germany). The only adjustments that were made during microscopy were rotation changes, brightness changes, contrast changes, and selection of the image size. The number of $A\beta_{42}$ and GFAP colocalization and non-colocalization was measured, and the ratio was calculated. The detailed antibody information is provided in **Table 1**.

Statistical analysis

No statistical methods were used to predetermine sample sizes; however, our sample sizes are similar to those reported in previous publications (Zhang et al., 2019; Luo et al., 2020). The loss rate of laboratory animals is about 4% due to anesthesia and natural death, and the lost animals were not included in the results. All data in this study are expressed as the mean ± standard error of mean (SEM). SPSS 26.0 (IBM, Chicago, IL, USA) and GraphPad Prism software v8 (GraphPad Software, La Jolla, CA, USA) were used for statistical analysis and graphing of data. Data from the Morris water maze hidden platform test were analyzed using repeated-measures analysis of variance, with escape latency and path length on four consecutive days as the repeated measures variables, and "group" (CTL, AD, ADS, or ADT) as the independent variable. Data from the other experiments were analyzed using one-way analysis of variance. Tukey's *post hoc* test was used to detect significant between-group differences. Statistical significance was defined as a P-value < 0.05.

Results

AtDCS improves the performance of APP/PS1 mice in the Morris water maze test

In the visible platform test, there was no significant between-group differences in escape latency (P > 0.05; **Figure 3A**) or path length (P > 0.05; **Figure 3B**), which indicates that there were no differences in visual acuity or motor ability between the groups. In the hidden platform test, the escape latency and path length of the mice in each group showed a downward trend over time, and there were significant main effects of group and day on path length and escape latency (group: both, P < 0.001; day: both, P < 0.001; **Figure 3C** and **D**). In the probe test, the CTL and ADT groups made significantly more platform crossings (all, P < 0.05; **Figure 3E**) and spent significantly more time in the target quadrant (all, P < 0.05; **Figure 3F**) than the AD and ADS groups. Additionally, the CTL and ADT groups spent significantly longer in the target quadrant than in the other quadrants (both, P < 0.001), but there was no significant difference in the time spent in the different quadrants in the AD and ADS groups (both, P > 0.05; **Figure 3G**). In both the hidden platform and probe tests, the performance of the ADT group was not significantly different from that of the CTL group (**Figure 3**).

AtDCS improves the preference of APP/PS1 mice in the novel object recognition and novel object location tests

The discrimination ratio (P < 0.001; **Figure 4A**) and location index (P < 0.005; **Figure 4B**) of the AD and ADS groups in the novel object recognition and novel object location tests, respectively, were significantly lower than those in the CTL group. The ADT group showed a higher discrimination ratio (P = 0.005) and location index (P < 0.001) than the AD and ADS groups. There were no significant differences between the CTL and ADT groups in discrimination ratio and location index (P > 0.05; **Figure 4**).

AtDCS reduces $A\beta_{42}$ levels in the hippocampus of APP/PS1 mice

The behavioral tests revealed no significant differences in performance between the ADS and AD groups, which indicates that the tDCS manipulation had no effect on behavior. Therefore, we performed histological evaluation in the CTL, AD, and ADT groups. Compared with the AD group, the ADT group showed a lower $A\beta_{42}$ protein level in the hippocampus 6 weeks after the end of AtDCS (P < 0.001; **Figure 5A**). $A\beta_{42}$ was not observed in the CTL group (**Figure 5B**). In the representative images of immunohistochemistry, the IOD of $A\beta_{42}$ in the hippocampus was greater in the AD group than that in the ADT group (**Figure 5C** and **D**). The IOD of $A\beta_{42}$ in the ADT group was significantly lower than that in the AD group (P < 0.001; **Figure 5E**).

AtDCS reduces inflammation levels in the hippocampus of APP/PS1 mice
The western blot results showed that the GFAP protein level in the hippocampus was significantly lower in the ADT group than in the AD group ($P < 0.001$), but also significantly higher in the ADT group than that in the CTL group ($P < 0.05$, **Figure 6A**). In the hippocampus, GFAP immunohistochemical staining was weaker in the ADT group than in the AD group, and there were fewer glial fibrils and protrusions in the ADT group. There was obviously more GFAP in the AD group than in the ADT group (**Figure 6B**). The IOD of GFAP in the three subregions of the hippocampus, i.e., the dentate gyrus (DG), CA2-3, and CA1, differed significantly between the three groups ($P < 0.001$; **Figure 6C**).

AtDCS protects hippocampal neurons in APP/PS1 mice
NeuN is a marker of mature neurons (Gusel'nikova and Korzhevskiy, 2015). The western blot results showed that the NeuN protein level of the CTL group was significantly higher than that of the AD group ($P < 0.001$) and ADT group ($P < 0.05$), and that the NeuN protein level in the ADT group was significantly higher than that in the AD group ($P < 0.05$; **Figure 7A**). In the hippocampus, the protein expression of caspase 3, which is related to apoptosis, was significantly downregulated in the ADT group compared with the AD group ($P < 0.001$; **Figure 7B**). Neurons in the CTL group were relatively intact and densely stained. However, neurons in the AD group were missing and sparse. Obviously intact neurons could be seen in the ADT group (**Figure 7C**). The IOD of NeuN in the three subregions of the hippocampus, i.e., the DG, CA2-3, and CA1, differed significantly between the three groups ($P < 0.005$; **Figure 7D**).

AtDCS regulates Aβ metabolism in the hippocampus of APP/PS1 mice
APP, β-site amyloid precursor protein cleaving enzyme 1 (BACE1), a disintegrin and metalloprotease domain 10 (ADAM10), neprilysin (NEP, also known as CD10), and insulin-degrading enzyme (IDE) are associated with Aβ metabolism (Yoon and Jo, 2012; Barage and Sonawane, 2015). The protein levels of APP and BACE1 in the hippocampus were significantly higher in the AD group than in the CTL group (both, $P < 0.001$), and the protein levels of ADAM10, CD10, and IDE were significantly lower (all $P < 0.001$). Among the APP/PS1 mice, APP and BACE1 protein levels in the hippocampus were significantly lower in the ADT group than in the AD group (both, $P < 0.001$), and the protein levels of ADAM10, CD10, and IDE were significantly higher (all, $P < 0.005$; **Figure 8**).

Colocalization of $A\beta_{42}$ and GFAP in the hippocampus of APP/PS1 mice
Consistent with the western blot and immunohistochemistry results, the confocal results showed that the GFAP level in the ADT group was lower than that in the AD group and higher than that in the CTL group. Since no $A\beta_{42}$ was observed in the CTL group, there was no green labeling in the CTL group under immunofluorescence (**Figure 9A**). The amount of green $A\beta_{42}$ in the ADT group was significantly less than that in the AD group, and the area of $A\beta_{42}$ was relatively small. Consistent with previous research (Itagaki et al., 1989; Luo et al., 2020), in which high expression levels of $A\beta_{42}$ were reported, high expression levels of GFAP were also found (**Figure 9B** and **C**). The colocalization of $A\beta_{42}$ and GFAP existed in both AD and ADT groups (**Figure 9B** and **C**). The ratio of this phenomenon in the ADT group was significantly higher than that in the AD group (**Figure 9D**).

Discussion

This study evaluated the long-term effect of AtDCS in a mouse model of preclinical AD. Six weeks after APP/PS1 mice in the preclinical stage of AD had been subjected to AtDCS, the mice showed improvements in cognitive ability and spatial learning and memory, the levels of Aβ and GFAP in the hippocampus were reduced, and neurons were relatively intact. These results indicate that the effect of AtDCS in APP/PS1 mice in the preclinical stage of AD can last at least 6 weeks. Thus, AtDCS is a promising treatment that might effectively delay the course of AD. In addition, this study also found that Aβ metabolism was improved in APP/PS1 mice after AtDCS, which indicates that AtDCS may effectively treat AD by regulating Aβ metabolism. The colocalization of Aβ and GFAP suggests that astrocytes play a crucial role in the long-term effect of AtDCS on the clinical course of AD.

Aβ is a typical pathological marker of the AD pathophysiological process (Barage and Sonawane, 2015; Chen et al., 2017), and spatial memory is one of the earliest affected functions (Gazova et al., 2012; Boccia et al., 2016). Previous studies have reported that, at the age of 6 months (approximately 26 weeks), APP/PS1 mice began to develop Aβ deposits in the hippocampus (Jankowsky et al., 2004; Zhang et al., 2007), exhibited significantly decreased NEP levels (Zhou et al., 2017), and began to show spatial memory defects (Luo et al., 2020). Thereafter, the Aβ level increased sharply, and recognition memory was impaired for about 30 weeks (Murphy et al., 2007; Zhang et al., 2007; Woo et al., 2010). According to the definition of the preclinical stage of AD (Sperling et al., 2011), 26-week-old APP/PS1 mice can be considered as being in the preclinical stage of AD. At 8 months (approximately 34 weeks) of age, the AD group considered to be in the clinical stage of AD showed spatial and recognition memory deficits, which is consistent with other studies (Woo et al., 2010; Cai et al., 2017). Therefore, we chose to subject mice to AtDCS at 26 weeks of age and to the Morris water maze, novel object recognition, and novel object location tests to assess spatial learning, memory, and recognition memory, respectively, at 34 weeks of age.

AtDCS can delay the progression of AD for at least 6 weeks
The 26-week-old APP/PS1 mice exhibited improvements in memory-related behavior 6 weeks after AtDCS. This improvement was reflected not only by the Morris water maze performance, but also by the discrimination ratio and location index in the novel object recognition and novel object location tests, respectively. Previous studies have reported that the Morris water maze performance of 26-week-old APP/PS1 mice improved immediately after AtDCS, and they did not show recognition memory deficits (Luo et al., 2020). This further verified that the mice were in the clinical stage of AD at 34 weeks of age. These results are direct evidence that AtDCS can delay the course of AD.

Histological analysis showed an improvement in the pathological status of the ADT group, which may be associated with the observed behavioral improvements. The amyloid hypothesis is the primary explanation for the pathogenesis of AD (Barage and Sonawane, 2015; Selkoe and Hardy, 2016). The neurotoxic properties of abnormal Aβ deposits lead to neuroinflammation, synaptic dysfunction, and neuronal damage and apoptosis (Sperling et al., 2011; Hughes et al., 2020). Aβ immunotherapy can prevent the cognitive deficits observed in AD model mice (Carrera et al., 2015) and reduce Aβ levels and inflammation (Sevigny et al., 2016). A reduction in the Aβ level is accompanied by a decrease in neuroinflammation and normalization of neurons, so it is not surprising that reducing the level of Aβ slows the progression of AD. Eight-month-old APP/PS1 mice exhibited high levels of Aβ in the hippocampus, severe inflammation, neuronal disorders, and impaired behavior, which is in line with the symptoms of AD. Twenty-six-week-old APP/PS1 mice in the preclinical stage of AD had significantly lower Aβ and GFAP levels after AtDCS and had relatively intact neurons (Luo et al., 2020). These parameters were the same in 26-week-old APP/PS1 mice and at 6 weeks after AtDCS. A reduction in Aβ levels induces long-term clinical benefits in AD mice in the preclinical stage (Sevigny et al., 2016). This finding once again verified that AtDCS had a profound effect on AD model mice in the preclinical stage at the histological level and that this persisted over time. However, it is unclear how AtDCS reduces Aβ levels.

AtDCS may reduce Aβ levels by regulating Aβ metabolism
The unbalanced production and degradation of Aβ lead to its abnormal accumulation. APP produces Aβ under the action of β-secretase (canonical β-secretase, BACE1) and γ-secretase (Chen et al., 2017; Patwardhan and Belemkar, 2021). A significant increase in BACE1 levels contributes to the production of Aβ (Cole and Vassar, 2007). ADAM10 is the main α-secretase of the nonamyloidogenic processing pathway of APP, which can limit the amyloidogenic processing of APP (Kuhn et al., 2010). It has been reported that higher levels of ADAM10 help reduce the formation of Aβ and increase the generation of the neuroprotective soluble N-terminal APP domain, which is released by α-secretase (Postina et al., 2004). In the ADT group, the levels of APP and BACE1 were decreased, and the levels of ADAM10 were increased, which indicates that AtDCS reduced the production of Aβ. CD10 and IDE are considered the main peptidases involved in the degradation of Aβ, and can promote the degradation and clearance of Aβ (Jha et al., 2015). In the ADT group, the levels of CD10 and IDE were increased, which suggests that AtDCS increased the degradation of Aβ. On the basis of this finding, we can speculate that AtDCS reduces the production of Aβ by promoting the nonamyloidogenic processing pathway and reducing the amyloidogenic processing pathway of APP, and increasing the degradation to reduce the abnormal deposition of Aβ, thereby slowing the course of AD. However, whether AtDCS directly or indirectly regulates Aβ metabolism needs to be verified by further studies.

AtDCS may reduce Aβ levels by participating in the regulation of glial cells
In the AD group, $A\beta_{42}$ and GFAP were colocalized, which is consistent with previous reports (Medeiros and LaFerla, 2013; Luo et al., 2020). Compared with the AD group, in the ADT group, the rate of this phenomenon increased significantly. GFAP is a marker of astrocyte activation (Benninger et al., 2016; Carter et al., 2019). Activated astrocytes function normally and can express Aβ-degrading enzymes to participate in the degradation and clearance of extracellular Aβ, act through the lysosomal system within astrocytes to engulf and degrade Aβ, or interact with neurons and capillary endothelial cells that form the blood-brain barrier to participate in the clearance of Aβ, thereby reducing the neurotoxicity caused by Aβ deposition *in vivo* (Wyss-Coray et al., 2003; Apátiga-Pérez et al., 2021; Price et al., 2021). However, astrocytes can accelerate the process of AD under pathological conditions. According to the two-hit hypothesis of AD, blood-brain barrier damage involving astrocytes disrupts the homeostasis of Aβ metabolism (Zlokovic, 2011), and the loss of receptors in astrocytes also reduces the clearance of Aβ (Basak et al., 2012), which implies that astrocyte-mediated inhibition of Aβ degradation is related to the accumulation of Aβ. AtDCS regulates astrocytes and can initially increase their activation (Wachter et al., 2011; Pikhovych et al., 2016). In this study, AtDCS regulated Aβ metabolism and reduced the levels of Aβ and GFAP. Therefore, it is possible that the reduction in Aβ plaques in APP/PS1 mice after AtDCS was mediated by astrocytes. AtDCS initially increases the number of astrocytes to promote Aβ clearance, thus reducing Aβ levels; in turn, this decrease in Aβ levels leads to a subsequent reduction in the number of astrocytes, thereby slowing down the development of AD. Further research is needed to reveal the mechanism underlying this process. In addition, in AD, astrocytes have a high resting level of Ca^{2+} and produce synchronous activity near Aβ plaques (Kuchibhotla et al., 2009). Ca^{2+} signaling dysfunction in astrocytes can promote the development of AD (Alzheimer's Association Calcium Hypothesis Workgroup, 2017; Gómez-Gonzalo et al., 2017). Whether AtDCS regulates astrocytes through calcium signaling requires further exploration.

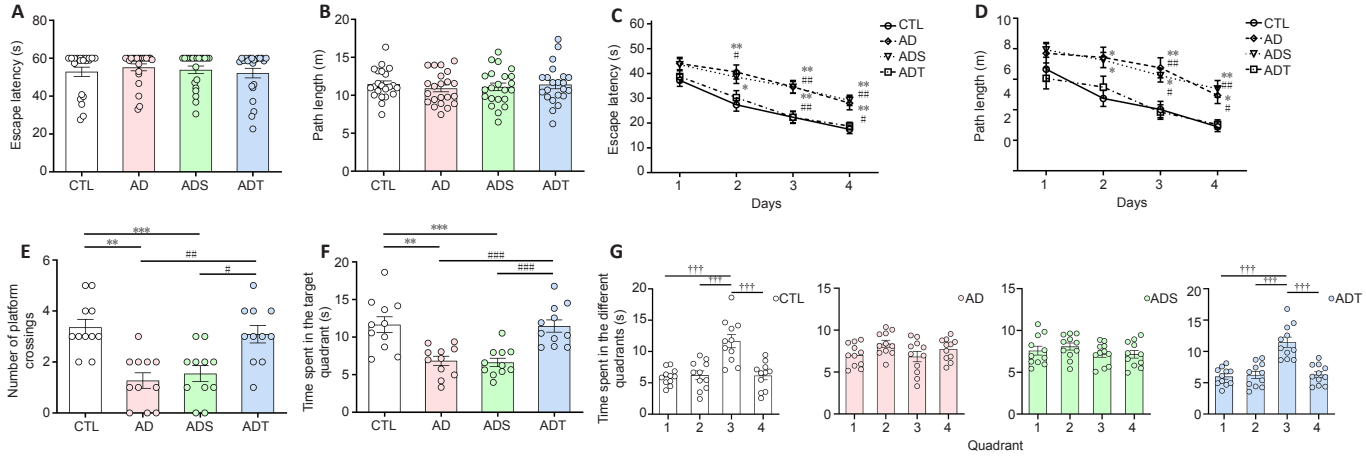

Figure 3 | **AtDCS improves the spatial learning and memory of APP/PS1 mice.**
(A, B) In the visible platform test, there was no significant difference in the escape latency (A) or path length (B) between the four groups. (C, D) In the hidden platform test, the escape latency (C) and path length (D) were significantly shorter in the ADT group than in the AD and ADS groups. (E–G) In the probe test, the number of platform crossings (E) in the ADT group was significantly higher than that in the AD and ADS groups, and the time spent in the target quadrant (F) was significantly longer. The CTL and ADT groups took significantly longer to recognize the target quadrant than the other three quadrants (G). Data are expressed as the mean ± SEM (n = 11 per group). Data from the hidden platform task were analyzed using a repeated-measures analysis of variance. Data from other experiments were analyzed using a one-way analysis of variance followed by Tukey's *post hoc* test. *P < 0.05, **P < 0.01, ***P < 0.001, *vs.* CTL group; #P < 0.05, ##P < 0.01, ###P < 0.001, *vs.* ADT group; †††P < 0.001, *vs.* the third quadrant. The detailed F- and P-values are shown in Additional Table 1. AD: APP/PS1; ADS: APP/PS1 + sham AtDCS; ADT: APP/PS1 + AtDCS; APP/PS1: APPswe/PSEN1dE9; AtDCS: anodal transcranial direct current stimulation; CTL: control.

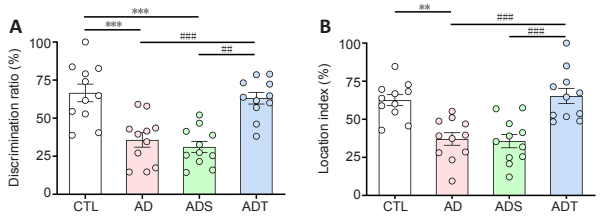

Figure 4 | **AtDCS improves the recognition memory of APP/PS1 mice.**
(A, B) Compared with the AD group and the ADS group, the ADT group had a significantly higher recognition index in the novel object recognition test (A) and location index in the novel location recognition test (B). A higher recognition index or position index score indicates better recognition memory. Data are expressed as the mean ± SEM (n = 11 per group). **P < 0.005, ***P < 0.001, *vs.* CTL group; ##P < 0.005, ###P < 0.001, *vs.* ADT group (one-way analysis of variance followed by Tukey's *post hoc* test). The detailed F- and P-values are shown in Additional Table 1. AD: APP/PS1; ADS: APP/PS1 + sham AtDCS; ADT: APP/PS1 + AtDCS; APP/PS1: APPswe/PSEN1dE9; AtDCS: anodal transcranial direct current stimulation; CTL: control.

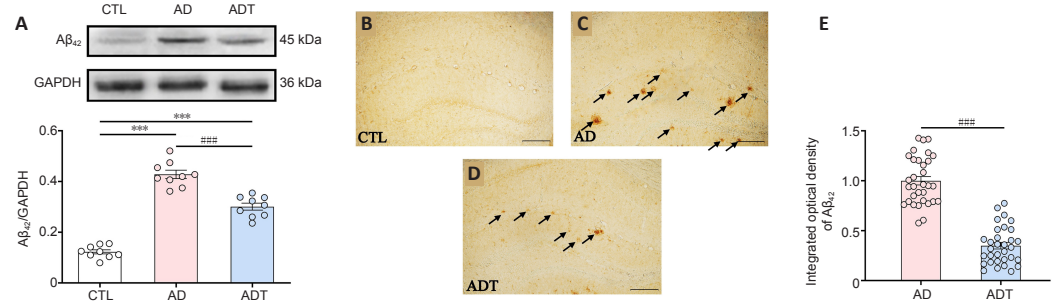

Figure 5 | **AtDCS reduces hippocampal Aβ_{42} levels in APP/PS1 mice.**
(A) Compared with the AD group, the Aβ_{42} protein level in the hippocampus was significantly decreased in the APP/PS1 mice 6 weeks after the end of AtDCS, as detected using western blot. (B–D) Representative immunohistochemical images of Aβ_{42} in the hippocampus. Aβ_{42} was not observed in the CTL group (B). (C, D) The number and area of Aβ_{42} plaques were greater in the AD group than in the ADT group. The black arrow points to Aβ_{42}. Scale bars: 500 μm. (E) Compared with AD group, the integrated optical density of Aβ_{42} in the ADT group was significantly reduced. Data are expressed as the mean ± SEM (n = 3 (western blot) or 8 (immunohistochemistry) per group). ***P < 0.001, *vs.* CTL group; ###P < 0.001, *vs.* ADT group (one-way analysis of variance followed by Tukey's *post hoc* test). The detailed F- and P-values are shown in Additional Table 2. Aβ_{42}: Amyloid-β42; AD: APP/PS1; ADT: APP/PS1 + AtDCS; APP/PS1: APPswe/PSEN1dE9; AtDCS: anodal transcranial direct current stimulation; CTL: control; GAPDH: glyceraldehyde-3-phosphate dehydrogenase.

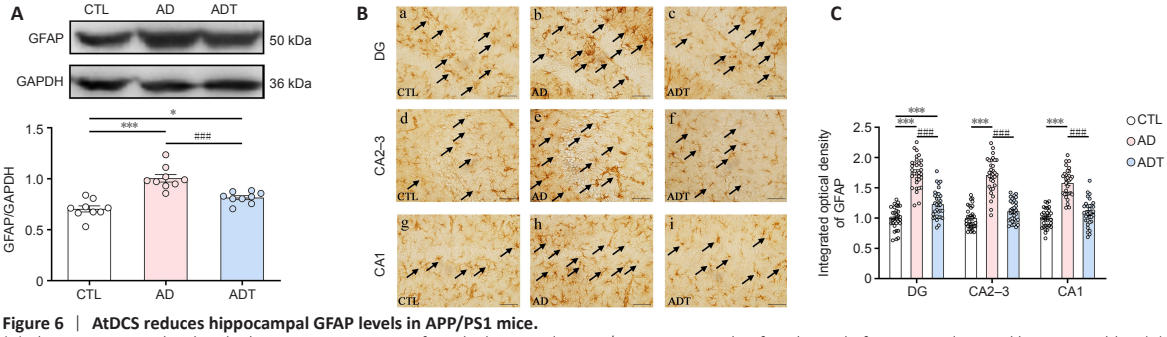

Figure 6 | **AtDCS reduces hippocampal GFAP levels in APP/PS1 mice.**
(A) The GFAP protein level in the hippocampus was significantly decreased in APP/PS1 mice 6 weeks after the end of AtDCS, as detected by western blot. (B) Representative immunohistochemical images of GFAP in the hippocampus. The CTL group and ADT group had deeper GFAP immunohistochemical staining and more glial fibrils and protrusions compared with the AD group. The black arrow points to GFAP. Scale bars: 200 μm. (C) Compared with that of the AD group, the integrated optical density of GFAP in the ADT group was significantly reduced. Data are expressed as the mean ± SEM (n = 3 (western blot) and 8 (immunohistochemistry) from each group). *P < 0.05, ***P < 0.001, *vs.* CTL group; ###P < 0.001, *vs.* ADT group (one-way analysis of variance followed by Tukey's *post hoc* test). The detailed F- and P-values are shown in Additional Table 2. AD: APP/PS1; ADT: APP/PS1 + AtDCS; APP/PS1: APPswe/PSEN1dE9; AtDCS: anodal transcranial direct current stimulation; CTL: control; DG: dentate gyrus; GAPDH: glyceraldehyde-3-phosphate dehydrogenase; GFAP: glial fibrillary acidic protein.

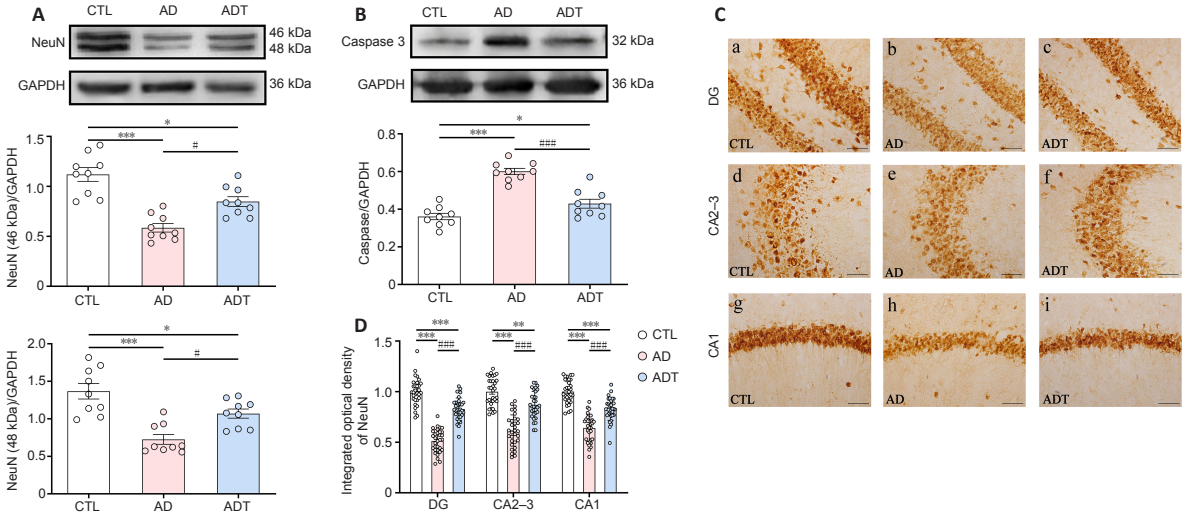

Figure 7 | **AtDCS protects hippocampal neurons in APP/PS1 mice.**
(A, B) The NeuN protein level was significantly decreased (A), and the protein level of caspase 3 was significantly downregulated (B) in the hippocampus of APP/PS1 mice 6 weeks after the end of AtDCS. (C) Representative immunohistochemical images of NeuN in the hippocampus. Neurons in the CTL group and ADT group were relatively intact and densely stained. Neurons in the AD group were missing and sparse. Scale bars: 200 μm. (D) Compared with that of the AD group, the integrated optical density of NeuN in the ADT group was significantly reduced. Data are expressed as the mean ± SEM (n = 3 (western blot) and 8 (immunohistochemistry) from each group). *P < 0.05, **P < 0.005, ***P < 0.001, *vs*. CTL group; #P < 0.05, ###P < 0.001, *vs*. ADT group (one-way analysis of variance followed by Tukey's *post hoc* test). The detailed F- and P-values are shown in Additional Table 2. AD: APP/PS1; ADT: APP/PS1 + AtDCS; APP/PS1: APPswe/PSEN1dE9; AtDCS: anodal transcranial direct current stimulation; CTL: control; DG: dentate gyrus; GAPDH: glyceraldehyde-3-phosphate dehydrogenase.

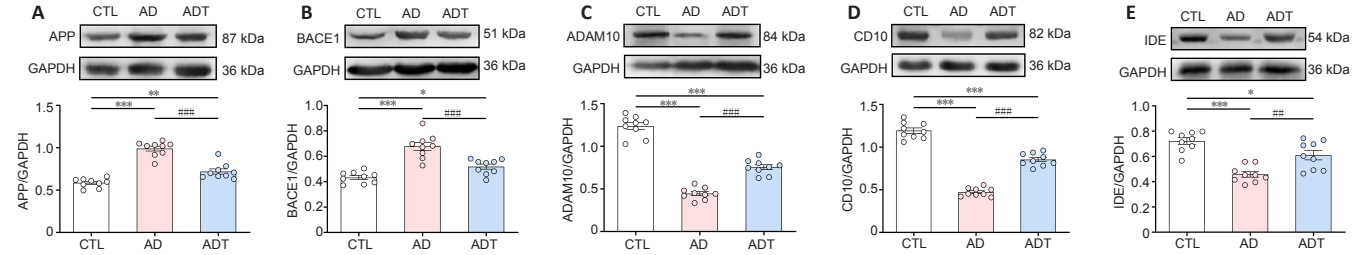

Figure 8 | **AtDCS regulates the metabolism of hippocampal Aβ in APP/PS1 mice.**
(A–E) In the hippocampus, the protein levels of APP (A) and BACE1 (B) were significantly decreased, and the protein levels of ADAM10 (C), CD10 (D), and IDE (E) were obviously increased in APP/PS1 mice 6 weeks after the end of AtDCS. Data are expressed as the mean ± SEM (n = 3 per group). *P < 0.05, **P < 0.005, ***P < 0.001, *vs*. CTL group; ##P < 0.005, ###P < 0.001, *vs*. ADT group (one-way analysis of variance followed by Tukey's *post hoc* test). The detailed F- and P-values are shown in Additional Table 2. AD: APP/PS1; ADAM10: A disintegrin and metalloprotease domain 10; ADT: APP/PS1 + AtDCS; APP: amyloid precursor protein; APP/PS1: APPswe/PSEN1dE9; AtDCS: anodal transcranial direct current stimulation; BACE1: β-site amyloid precursor protein cleaving enzyme 1; CD10: Neprilysin; CTL: control; DG: dentate gyrus; GAPDH: glyceraldehyde-3-phosphate dehydrogenase; IDE: insulin-degrading enzyme.

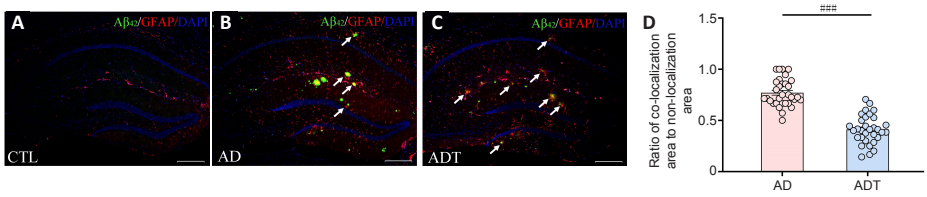

Figure 9 | **Results of double immunofluorescence staining for Aβ and GFAP in the hippocampus in the three groups.**
(A) No $A\beta_{42}$ was observed in the CTL group. (B, C) The white arrows point to the colocalization areas of $A\beta_{42}$ (green, Alexa Fluor 488) and GFAP (red, Alexa Fluor 594). The colocalization of $A\beta_{42}$ and GFAP (arrows) in the ADT group was more obvious than that in the AD group. Scale bars: 500 μm. (D) The ratio of colocalization of $A\beta_{42}$ and GFAP in the ADT group was significantly higher than that in the AD group. Data are expressed as the mean ± SEM (n = 8 per group). ###P < 0.001, *vs*. ADT group (one-way analysis of variance followed by Tukey's *post hoc* test). The detailed F- and P-values are shown in Additional Table 2. $A\beta_{42}$: Amloid-β42; AD: APP/PS1; ADT: APP/PS1 + AtDCS; APP/PS1: APPswe/PSEN1dE9; AtDCS: anodal transcranial direct current stimulation; CTL: control; DAPI: 4′,6-diamidino-2-phenylindole; GFAP: glial fibrillary acidic protein.

AtDCS may reduce Aβ levels through exerting a neuroprotective effect

Apoptosis leads to an increase in Aβ levels, and neuronal damage is one of the potential mechanisms underlying AD (Cotman and Su, 1996; Gervais et al., 1999). Some studies have confirmed that caspase 3 is activated during Aβ-induced neuronal apoptosis (Chang et al., 2016) and that caspase 3 immunoreactivity is activated in patients with AD (Bredesen et al., 2006) and in animal models of AD (Li et al., 2020). Upregulation of caspase 3 expression can exacerbate the proteolysis of APP, resulting in the production of high levels of cytotoxic Aβ peptides and leading to Aβ-induced neuronal stress (Gervais et al., 1999). tDCS has been shown to exert neuroprotective effects in animal models of ischemic stroke (Zhang et al., 2020). In the animal model of AD used in the present study, AtDCS decreased the levels of caspase 3 and APP, increased the level of NeuN, and maintained the integrity of neurons, which suggests that AtDCS may reduce the production of Aβ by inhibiting the apoptosis pathway and exerting a neuroprotective effect. During AtDCS, membrane depolarization is accompanied by the activation of Ca^{2+} channels. Ca^{2+} channel blockers can eliminate the long-term effect of AtDCS (Nitsche et al., 2003). It remains unknown whether the neuroprotective effect of AtDCS is related to Ca^{2+} signaling.

The stimulation parameters of tDCS, such as stimulation polarity, stimulation target, stimulation cycle, and charge density (current intensity × duration/electrode size), are highly heterogeneous across different studies, which will inevitably lead to different effects of the treatment on AD (Ciullo et al., 2021). In most studies, AtDCS has been demonstrated to bring more benefits than cathode tDCS in the treatment of patients with AD and animal models of AD (Yu et al., 2015; Luo et al., 2020; Gangemi et al., 2021). The frontal cortex, which was the target of tDCS in this study, is closely related to working memory (Owen et al., 1996; Wager and Smith, 2003). tDCS over the frontal cortex can improve the spatial learning and memory of APP/PS1 mice in the preclinical stage of AD, and the visual recognition and memory of patients with AD. The repeated tDCS cycle is based on tDCS treatment over the frontal cortex in people with depression (Boggio et al., 2008). These studies indicates that the frontal cortex could be a potential target for tDCS in the treatment of AD. Although our charge density (85.987 kC/m^2) is safe for use in mice (Pikhovych et al., 2016), due to the differences in the physiological systems of humans and animals, the charge density parameters cannot be recommended for clinical applications.

Our research has some limitations. This work only examined the treatment benefit 6 weeks after receiving two weeks of AtDCS treatment. It is not clear how long this treatment benefit lasts, or whether the effect after treatment is

affected by the length of treatment. It is also unknown how AtDCS reduces Aβ metabolism and glial cell expression. The role of AtDCS in the preclinical stage of AD is complex, and its mechanism involves various regulatory processes *in vivo*. It is necessary to study the relationship between Ca^{2+} signaling, glial cells, and Aβ metabolism to further elucidate the mechanism of AtDCS in AD treatment. Due to the wide phylogenetic gap between mice and humans with AD, the application of AtDCS in the preclinical stage of AD still needs continuous exploration.

In conclusion, our results show that the effect of AtDCS persisted for at least 6 weeks in APP/PS1 mice, which provides new insights into the mechanisms underlying the preventive and therapeutic effects of AtDCS in the preclinical stage of AD.

Author contributions: *Study design: YPL, XLT, HZW; experiment implementation:YPL, ZL, CW, XFY, HZW; data analysis: YPL, ZL, CW, XFY; manuscript drafting: YPL, XYW, HZW; manuscript revision: YPL, ZL, CW, XFY, XYW, XLT, HZW. All authors have read and approved the final manuscript.*
Conflicts of interest: *The authors have no conflict of interest to report.*
Availability of data and materials: *All data generated or analyzed during this study are included in this published article and its supplementary information files.*

Open peer reviewer: *John Noel Viaña, Australian National University, Australia.*
Additional files:
Additional Table 1: *F- and P-values in behavioral experiments.*
Additional Table 2: *F- and P-values in western blot, immunohistochemistry, and immunofluorescence.*
Additional file 1: *Open peer review report 1.*

References

Alzheimer's Association Calcium Hypothesis Workgroup (2017) Calcium Hypothesis of Alzheimer's disease and brain aging: A framework for integrating new evidence into a comprehensive theory of pathogenesis. Alzheimers Dement 13:178-182.e17.

Antunes M, Biala G (2012) The novel object recognition memory: neurobiology, test procedure, and its modifications. Cogn Process 13:93-110.

Apátiga-Pérez R, Soto-Rojas LO, Campa-Córdoba BB, Luna-Viramontes NI, Cuevas E, Villanueva-Fierro I, Ontiveros-Torres MA, Bravo-Muñoz M, Flores-Rodríguez P, Garcés-Ramirez L, de la Cruz F, Montiel-Sosa JF, Pacheco-Herrero M, Luna-Muñoz J (2021) Neurovascular dysfunction and vascular amyloid accumulation as early events in Alzheimer's disease. Metab Brain Dis doi: 10.1007/s11011-021-00814-4.

Aranda MP, Kremer IN, Hinton L, Zissimopoulos J, Whitmer RA, Hummel CH, Trejo L, Fabius C (2021) Impact of dementia: Health disparities, population trends, care interventions, and economic costs. J Am Geriatr Soc 69:1774-1783.

Barage SH, Sonawane KD (2015) Amyloid cascade hypothesis: pathogenesis and therapeutic strategies in Alzheimer's disease. Neuropeptides 52:1-18.

Basak JM, Verghese PB, Yoon H, Kim J, Holtzman DM (2012) Low-density lipoprotein receptor represents an apolipoprotein E-independent pathway of Aβ uptake and degradation by astrocytes. J Biol Chem 287:13959-13971.

Bello-Arroyo E, Roque H, Marcos A, Orihuel J, Higuera-Matas A, Desco M, Caiolfa VR, Ambrosio E, Lara-Pezzi E, Gómez-Gaviro MV (2018) MouBeAT: a new and open toolbox for guided analysis of behavioral tests in mice. Front Behav Neurosci 12:201.

Benninger F, Glat MJ, Offen D, Steiner I (2016) Glial fibrillary acidic protein as a marker of astrocytic activation in the cerebrospinal fluid of patients with amyotrophic lateral sclerosis. J Clin Neurosci 26:75-78.

Boccia M, Silveri MC, Sabatini U, Guariglia C, Nemmi F (2016) Neural underpinnings of the decline of topographical memory in mild cognitive impairment. Am J Alzheimers Dis Other Demen 31:618-630.

Boggio PS, Rigonatti SP, Ribeiro RB, Myczkowski ML, Nitsche MA, Pascual-Leone A, Fregni F (2008) A randomized, double-blind clinical trial on the efficacy of cortical direct current stimulation for the treatment of major depression. Int J Neuropsychopharmacol 11:249-254.

Bredesen DE, Rao RV, Mehlen P (2006) Cell death in the nervous system. Nature 443:796-802.

Cai H, Wang Y, He J, Cai T, Wu J, Fang J, Zhang R, Guo Z, Guan L, Zhan Q, Lin L, Xiao Y, Pan H, Wang Q (2017) Neuroprotective effects of bajijiasu against cognitive impairment induced by amyloid-β in APP/PS1 mice. Oncotarget 8:92621-92634.

Carrera I, Etcheverría I, Fernández-Novoa L, Lombardi VR, Lakshmana MK, Cacabelos R, Vigo C (2015) A comparative evaluation of a novel vaccine in APP/PS1 mouse models of Alzheimer's disease. Biomed Res Int 2015:807146.

Carter SF, Herholz K, Rosa-Neto P, Pellerin L, Nordberg A, Zimmer ER (2019) Astrocyte biomarkers in Alzheimer's disease. Trends Mol Med 25:77-95.

Chang YJ, Linh NH, Shih YH, Yu HM, Li MS, Chen YR (2016) Alzheimer's amyloid-β sequesters caspase-3 in vitro via its C-terminal tail. ACS Chem Neurosci 7:1097-1106.

Chen GF, Xu TH, Yan Y, Zhou YR, Jiang Y, Melcher K, Xu HE (2017) Amyloid beta: structure, biology and structure-based therapeutic development. Acta Pharmacol Sin 38:1205-1235.

Ciullo V, Spalletta G, Caltagirone C, Banaj N, Vecchio D, Piras F, Piras F (2021) Transcranial direct current stimulation and cognition in neuropsychiatric disorders: systematic review of the evidence and future directions. Neuroscientist 27:285-309.

Cole SL, Vassar R (2007) The Alzheimer's disease beta-secretase enzyme, BACE1. Mol Neurodegener 2:22.

Cotman CW, Su JH (1996) Mechanisms of neuronal death in Alzheimer's disease. Brain Pathol 6:493-506.

Esquerda-Canals G, Montoliu-Gaya L, Güell-Bosch J, Villegas S (2017) Mouse models of Alzheimer's disease. J Alzheimers Dis 57:1171-1183.

Fakhoury M (2018) Microglia and astrocytes in Alzheimer's disease: implications for therapy. Curr Neuropharmacol 16:508-518.

Gangemi A, Colombo B, Fabio RA (2021) Effects of short- and long-term neurostimulation (tDCS) on Alzheimer's disease patients: two randomized studies. Aging Clin Exp Res 33:383-390.

Gazova I, Vlcek K, Laczó J, Nedelska Z, Hyncicova E, Mokrisova I, Sheardova K, Hort J (2012) Spatial navigation-a unique window into physiological and pathological aging. Front Aging Neurosci 4:16.

Gervais FG, Xu D, Robertson GS, Vaillancourt JP, Zhu Y, Huang J, LeBlanc A, Smith D, Rigby M, Shearman MS, Clarke EE, Zheng H, Van Der Ploeg LH, Ruffolo SC, Thornberry NA, Xanthoudakis S, Zamboni RJ, Roy S, Nicholson DW (1999) Involvement of caspases in proteolytic cleavage of Alzheimer's amyloid-beta precursor protein and amyloidogenic A beta peptide formation. Cell 97:395-406.

Gómez-Gonzalo M, Martin-Fernandez M, Martínez-Murillo R, Mederos S, Hernández-Vivanco A, Jamison S, Fernandez AP, Serrano J, Calero P, Futch HS, Corpas R, Sanfeliu C, Perea G, Araque A (2017) Neuron-astrocyte signaling is preserved in the aging brain. Glia 65:569-580.

Gusel'nikova VV, Korzhevskiy DE (2015) NeuN as a neuronal nuclear antigen and neuron differentiation marker. Acta Naturae 7:42-47.

Gutierrez MEZ, Savall ASP, da Luz Abreu E, Nakama KA, Dos Santos RB, Guedes MCM, Ávila DS, Luchese C, Haas SE, Quines CB, Pinton S (2021) Co-nanoencapsulated meloxicam and curcumin improves cognitive impairment induced by amyloid-beta through modulation of cyclooxygenase-2 in mice. Neural Regen Res 16:783-789.

Hughes C, Choi ML, Yi JH, Kim SC, Drews A, George-Hyslop PS, Bryant C, Gandhi S, Cho K, Klenerman D (2020) Beta amyloid aggregates induce sensitised TLR4 signalling causing long-term potentiation deficit and rat neuronal cell death. Commun Biol 3:79.

Itagaki S, McGeer PL, Akiyama H, Zhu S, Selkoe D (1989) Relationship of microglia and astrocytes to amyloid deposits of Alzheimer disease. J Neuroimmunol 24:173-182.

Jack CR, Jr., Bennett DA, Blennow K, Carrillo MC, Dunn B, Haeberlein SB, Holtzman DM, Jagust W, Jessen F, Karlawish J, Liu E, Molinuevo JL, Montine T, Phelps C, Rankin KP, Rowe CC, Scheltens P, Siemers E, Snyder HM, Sperling R (2018) NIA-AA Research Framework: toward a biological definition of Alzheimer's disease. Alzheimers Dement 14:535-562.

Jankowsky JL, Fadale DJ, Anderson J, Xu GM, Gonzales V, Jenkins NA, Copeland NG, Lee MK, Younkin LH, Wagner SL, Younkin SG, Borchelt DR (2004) Mutant presenilins specifically elevate the levels of the 42 residue beta-amyloid peptide in vivo: evidence for augmentation of a 42-specific gamma secretase. Hum Mol Genet 13:159-170.

Jha NK, Jha SK, Kumar D, Kejriwal N, Sharma R, Ambasta RK, Kumar P (2015) Impact of insulin degrading enzyme and neprilysin in Alzheimer's disease biology: characterization of putative cognates for therapeutic applications. J Alzheimers Dis 48:891-917.

Khedr EM, Gamal NF, El-Fetoh NA, Khalifa H, Ahmed EM, Ali AM, Noaman M, El-Baki AA, Karim AA (2014) A double-blind randomized clinical trial on the efficacy of cortical direct current stimulation for the treatment of Alzheimer's disease. Front Aging Neurosci 6:275.

Kuchibhotla KV, Lattarulo CR, Hyman BT, Bacskai BJ (2009) Synchronous hyperactivity and intercellular calcium waves in astrocytes in Alzheimer mice. Science 323:1211-1215.

Kuhn PH, Wang H, Dislich B, Colombo A, Zeitschel U, Ellwart JW, Kremmer E, Rossner S, Lichtenthaler SF (2010) ADAM10 is the physiologically relevant, constitutive alpha-secretase of the amyloid precursor protein in primary neurons. EMBO J 29:3020-3032.

Lee JC, Kim SJ, Hong S, Kim Y (2019) Diagnosis of Alzheimer's disease utilizing amyloid and tau as fluid biomarkers. Exp Mol Med 51:1-10.

Li J, Li D, Zhou H, Wu G, He Z, Liao W, Li Y, Zhi Y (2020) MicroRNA-338-5p alleviates neuronal apoptosis via directly targeting BCL2L11 in APP/PS1 mice. Aging (Albany NY) 12:20728-20742.

Lu H, Chan SSM, Chan WC, Lin C, Cheng CPW, Linda Chiu Wa L (2019) Randomized controlled trial of TDCS on cognition in 201 seniors with mild neurocognitive disorder. Ann Clin Transl Neurol 6:1938-1948.

Luo Y, Yang W, Li N, Yang X, Zhu B, Wang C, Hou W, Wang X, Wen H, Tian X (2020) Anodal transcranial direct current stimulation can improve spatial learning and memory and attenuate Aβ(42) burden at the early stage of Alzheimer's disease in APP/PS1 transgenic mice. Front Aging Neurosci 12:134.

Martorell AJ, Paulson AL, Suk HJ, Abdurrob F, Drummond GT, Guan W, Young JZ, Kim DN, Kritskiy O, Barker SJ, Mangena V, Prince SM, Brown EN, Chung K, Boyden ES, Singer AC, Tsai LH (2019) Multi-sensory gamma stimulation ameliorates Alzheimer's-associated pathology and improves cognition. Cell 177:256-271. e22.

Medeiros R, LaFerla FM (2013) Astrocytes: conductors of the Alzheimer disease neuroinflammatory symphony. Exp Neurol 239:133-138.

Murphy MP, Beckett TL, Ding Q, Patel E, Markesbery WR, St Clair DK, LeVine H, 3rd, Keller JN (2007) Abeta solubility and deposition during AD progression and in APPxPS-1 knock-in mice. Neurobiol Dis 27:301-311.

Mycroft-West CJ, Devlin AJ, Cooper LC, Procter P, Miller GJ, Fernig DG, Guerrini M, Guimond SE, Lima MA, Yates EA, Skidmore MA (2020) Inhibition of BACE1, the β-secretase implicated in Alzheimer's disease, by a chondroitin sulfate extract from Sardina pilchardus. Neural Regen Res 15:1546-1553.

Nitsche MA, Paulus W (2000) Excitability changes induced in the human motor cortex by weak transcranial direct current stimulation. J Physiol 527 Pt 3:633-639.

Nitsche MA, Fricke K, Henschke U, Schlitterlau A, Liebetanz D, Lang N, Henning S, Tergau F, Paulus W (2003) Pharmacological modulation of cortical excitability shifts induced by transcranial direct current stimulation in humans. J Physiol 553:293-301.

Owen AM, Evans AC, Petrides M (1996) Evidence for a two-stage model of spatial working memory processing within the lateral frontal cortex: a positron emission tomography study. Cereb Cortex 6:31-38.

Patwardhan AG, Belemkar S (2021) An update on Alzheimer's disease: Immunotherapeutic agents, stem cell therapy and gene editing. Life Sci 282:119790.

Percie du Sert N, Ahluwalia A, Alam S, Avey MT, Baker M, Browne WJ, Clark A, Cuthill IC, Dirnagl U, Emerson M, Garner P, Holgate ST, Howells DW, Hurst V, Karp NA, Lazic SE, Lidster K, MacCallum CJ, Macleod M, Pearl EJ, et al. (2020) Reporting animal research: explanation and elaboration for the ARRIVE guidelines 2.0. PLoS Biol 18:e3000411.

Pikhovych A, Stolberg NP, Jessica Flitsch L, Walter HL, Graf R, Fink GR, Schroeter M, Rueger MA (2016) Transcranial direct current stimulation modulates neurogenesis and microglia activation in the mouse brain. Stem Cells Int 2016:2715196.

Porsteinsson AP, Isaacson RS, Knox S, Sabbagh MN, Rubino I (2021) Diagnosis of early Alzheimer's disease: clinical practice in 2021. J Prev Alzheimers Dis 8:371-386.

Postina R, Schroeder A, Dewachter I, Bohl J, Schmitt U, Kojro E, Prinzen C, Endres K, Hiemke C, Blessing M, Flamez P, Dequenne A, Godaux E, van Leuven F, Fahrenholz F (2004) A disintegrin-metalloproteinase prevents amyloid plaque formation and hippocampal defects in an Alzheimer disease mouse model. J Clin Invest 113:1456-1464.

Price BR, Johnson LA, Norris CM (2021) Reactive astrocytes: The nexus of pathological and clinical hallmarks of Alzheimer's disease. Ageing Res Rev 68:101335.

Radaghdam S, Karamad V, Nourazarian A, Shademan B, Khaki-Khatibi F, Nikanfar M (2021) Molecular mechanisms of sex hormones in the development and progression of Alzheimer's disease. Neurosci Lett 764:136221.

Ryan NS, Rossor MN (2011) Defining and describing the pre-dementia stages of familial Alzheimer's disease. Alzheimers Res Ther 3:29.

Selkoe DJ, Hardy J (2016) The amyloid hypothesis of Alzheimer's disease at 25 years. EMBO Mol Med 8:595-608.

Sevigny J, Chiao P, Bussière T, Weinreb PH, Williams L, Maier M, Dunstan R, Salloway S, Chen T, Ling Y, O'Gorman J, Qian F, Arastu M, Li M, Chollate S, Brennan MS, Quintero-Monzon O, Scannevin RH, Arnold HM, Engber T, et al. (2016) The antibody aducanumab reduces Aβ plaques in Alzheimer's disease. Nature 537:50-56.

Sperling RA, Aisen PS, Beckett LA, Bennett DA, Craft S, Fagan AM, Iwatsubo T, Jack CR, Jr., Kaye J, Montine TJ, Park DC, Reiman EM, Rowe CC, Siemers E, Stern Y, Yaffe K, Carrillo MC, Thies B, Morrison-Bogorad M, Wagster MV, et al. (2011) Toward defining the preclinical stages of Alzheimer's disease: recommendations from the National Institute on Aging-Alzheimer's Association workgroups on diagnostic guidelines for Alzheimer's disease. Alzheimers Dement 7:280-292.

Stagg CJ, Nitsche MA (2011) Physiological basis of transcranial direct current stimulation. Neuroscientist 17:37-53.

Sun H, Liu M, Sun T, Chen Y, Lan Z, Lian B, Zhao C, Liu Z, Zhang J, Liu Y (2019) Age-related changes in hippocampal AD pathology, actin remodeling proteins and spatial memory behavior of male APP/PS1 mice. Behav Brain Res 376:112182.

Verkhratsky A, Olabarria M, Noristani HN, Yeh CY, Rodriguez JJ (2010) Astrocytes in Alzheimer's disease. Neurotherapeutics 7:399-412.

Villemagne VL, Burnham S, Bourgeat P, Brown B, Ellis KA, Salvado O, Szoeke C, Macaulay SL, Martins R, Maruff P, Ames D, Rowe CC, Masters CL (2013) Amyloid β deposition, neurodegeneration, and cognitive decline in sporadic Alzheimer's disease: a prospective cohort study. Lancet Neurol 12:357-367.

Wachter D, Wrede A, Schulz-Schaeffer W, Taghizadeh-Waghefi A, Nitsche MA, Kutschenko A, Rohde V, Liebetanz D (2011) Transcranial direct current stimulation induces polarity-specific changes of cortical blood perfusion in the rat. Exp Neurol 227:322-327.

Wager TD, Smith EE (2003) Neuroimaging studies of working memory: a meta-analysis. Cogn Affect Behav Neurosci 3:255-274.

Wang P, Sui HJ, Li XJ, Bai LN, Bi J, Lai H (2021) Melatonin ameliorates microvessel abnormalities in the cerebral cortex and hippocampus in a rat model of Alzheimer's disease. Neural Regen Res 16:757-764.

Woo DC, Lee SH, Lee DW, Kim SY, Kim GY, Rhim HS, Choi CB, Kim HY, Lee CU, Choe BY (2010) Regional metabolic alteration of Alzheimer's disease in mouse brain expressing mutant human APP-PS1 by 1H HR-MAS. Behav Brain Res 211:125-131.

Wyss-Coray T, Loike JD, Brionne TC, Lu E, Anankov R, Yan F, Silverstein SC, Husemann J (2003) Adult mouse astrocytes degrade amyloid-beta in vitro and in situ. Nat Med 9:453-457.

Yang WJ, Wen HZ, Zhou LX, Luo YP, Hou WS, Wang X, Tian XL (2019) After-effects of repetitive anodal transcranial direct current stimulation on learning and memory in a rat model of Alzheimer's disease. Neurobiol Learn Mem 161:37-45.

Yoon SS, Jo SA (2012) Mechanisms of amyloid-β peptide clearance: potential therapeutic targets for Alzheimer's disease. Biomol Ther (Seoul) 20:245-255.

Yu X, Li Y, Wen H, Zhang Y, Tian X (2015) Intensity-dependent effects of repetitive anodal transcranial direct current stimulation on learning and memory in a rat model of Alzheimer's disease. Neurobiol Learn Mem 123:168-178.

Zhang C, McNeil E, Dressler L, Siman R (2007) Long-lasting impairment in hippocampal neurogenesis associated with amyloid deposition in a knock-in mouse model of familial Alzheimer's disease. Exp Neurol 204:77-87.

Zhang KY, Rui G, Zhang JP, Guo L, An GZ, Lin JJ, He W, Ding GR (2020) Cathodal tDCS exerts neuroprotective effect in rat brain after acute ischemic stroke. BMC Neurosci 21:21.

Zhang YY, Liu MY, Liu Z, Zhao JK, Zhao YG, He L, Li W, Zhang JQ (2019) GPR30-mediated estrogenic regulation of actin polymerization and spatial memory involves SRC-1 and PI3K-mTORC2 in the hippocampus of female mice. CNS Neurosci Ther 25:714-733.

Zhou L, Liu J, Dong D, Wei C, Wang R (2017) Dynamic alteration of neprilysin and endothelin-converting enzyme in age-dependent APPswe/PS1dE9 mouse model of Alzheimer's disease. Am J Transl Res 9:184-196.

Zhu S, Wang J, Zhang Y, He J, Kong J, Wang JF, Li XM (2017) The role of neuroinflammation and amyloid in cognitive impairment in an APP/PS1 transgenic mouse model of Alzheimer's disease. CNS Neurosci Ther 23:310-320.

Zlokovic BV (2011) Neurovascular pathways to neurodegeneration in Alzheimer's disease and other disorders. Nat Rev Neurosci 12:723-738.

P-Reviewer: Viaña JN; C-Editor: Zhao M; S-Editors: Yu J, Li CH; L-Editors: Cason N, Yu J, Song LP; T-Editor: Jia Y

Additional Table 1 *F*- and *P*-values in behavioral experiments

Experiment	Variable	Degrees of freedom	*F*-value	*P*-value
Morris water maze test				
Visible platform test	Escape latency			
	Group	3	0.532	0.661
	Path length			
	Group	3	0.299	0.826
Hidden platform test	Escape latency			
	Group	3	21.817	< 0.001
	Day	3	39.113	< 0.001
	Group* Day	9	0.532	0.852
	Path length			
	Group	3	17.070	< 0.001
	Day	3	21.717	< 0.001
	Group* Day	9	0.492	0.881
Probe test	Crossing			
	Group	3	11.175	< 0.001
	Retention time			
	Group	3	12.723	< 0.001
	quadrant			
	CTL	3	14.379	< 0.001
	AD	3	2.263	0.096
	ADS	3	0.904	0.447
	ADT	3	20.291	< 0.001
Novel object recognition test	Discrimination ration			
	Group	3	15.739	< 0.001
Novel object location test	Location index			
	Group	3	13.677	< 0.001

The data from the hidden platform task were analyzed by repeated measures analysis of variance. The data of other experiments were analyzed by one-way analysis of variance followed by Tukey's post hoc test. AD: APP/PS1; ADS: APP/PS1 + sham AtDCS; ADT: APP/PS1 + AtDCS; APP/PS1: APPswe/PSEN1dE9; CTL: control.

Additional Table 2 *F*- and *P*-values in western blot, immunohistochemistry, and immunofluorescence

Protein	Experiment	Variable	Degrees of freedom	*F*-value	*P*-value
$A\beta_{42}$	Western blot	$A\beta_{42}$/GAPDH			
		Group	2	134.505	< 0.001
	Immunohistochemistry	IOD			
		Group	1	146.599	< 0.001
GFAP	Western blot	GFAP/GAPDH			
		Group	2	26.807	< 0.001
	Immunohistochemistry	IOD of DG			
		Group	2	97.955	< 0.001
		IOD of CA2-3			
		Group	2	92.947	< 0.001
		IOD of CA1			
		Group	2	76.224	< 0.001
NeuN	Western blot	$NeuN_{46}$/GAPDH			
		Group	2	23.677	< 0.001
		$NeuN_{48}$/GAPDH			
		Group	2	16.460	<0.001
	Immunohistochemistry	IOD of DG			
		Group	2	135.840	< 0.001
		IOD of CA2-3			
		Group	2	60.880	< 0.001
		IOD of CA1			
		Group	2	71.139	< 0.001
Caspase 3	Western blot	Caspase 3/GAPDH			
		Group	2	41.736	< 0.001
APP	Western blot	APP/GAPDH			
		Group	2	62.117	< 0.001
BACE1	Western blot	BACE1/GAPDH			
		Group	2	28.623	< 0.001
ADAM10	Western blot	ADAM10/GAPDH			
		Group	2	157.896	< 0.001
CD10	Western blot	CD10/GAPDH			
		Group	2	204.403	< 0.001
IDE	Western blot	IDE/GAPDH			
		Group	2	20.995	< 0.001
$A\beta_{42}$ & GFAP	Immunofluorescence	Ratio of co-localization to non-localization			
		Group	1	112.255	< 0.001

The data were analyzed by one-way analysis of variance followed by Tukey's post hoc test. $A\beta_{42}$: Amyloid-β_{42}; ADAM10: a disintegrin and metalloprotease domain 10; APP: amyloid precursor protein; BACE1: β-site amyloid precursor protein cleaving enzyme 1; CD10: Neprilysin; DG: dentate gyrus; GAPDH: glyceraldehyde-3-phosphate dehydrogenase; GFAP: glial fibrillary acidic protein; IDE: insulin-degrading enzyme; IOD: integrated optical density.